JACS
JOURNAL OF THE AMERICAN CHEMICAL SOCIETY
Communication
pubs.acs.org/JACS

# Plasmon-Enhanced Photothermoelectric Conversion in Chemical Vapor Deposited Graphene p−n Junctions

Di Wu, Kai Yan, Yu Zhou, Huan Wang, Li Lin, Hailin Peng,* and Zhongfan Liu*

Center for Nanochemistry, Beijing National Laboratory for Molecular Sciences (BNLMS), State Key Laboratory for Structural Chemistry of Unstable and Stable Species, College of Chemistry and Molecular Engineering, Peking University, Beijing 100871, P.R. China

Supporting Information

**ABSTRACT:** Graphene p−n junctions grown by chemical vapor deposition hold great promise for the applications in high-speed, broadband photodetectors and energy conversion devices, where efficient photoelectric conversion can be realized by a hot-carrier-assisted photothermoelectric (PTE) effect and hot-carrier multiplication. However, the overall quantum efficiency is restricted by the low light absorption of single-layer graphene. Here, we present the first experimental demonstration of a plasmon-enhanced PTE conversion in chemical vapor deposited graphene p−n junctions. Surface plasmons of metallic nanostructures placed near the graphene p−n junctions were found to significantly enhance the optical field in the active layer and allow for a 4-fold increase in the photocurrent. Moreover, the utilization of localized plasmon enhancement facilitates the realization of efficient PTE conversion of graphene p−n junction devices under global illumination, which may offer an avenue for practical applications of graphene-based photodetectors and solar cells.

Graphene-based electronic and photonic devices with new design principles[1] or novel mechanisms[2] are constantly emerging, due to the combination of the exceptional electronic and optoelectronic properties of graphene which originate from its unique band structure. Particularly, the ultrahigh carrier mobility,[3] broadband light absorption,[4] and exceptional mechanical flexibility[5] make graphene an excellent candidate material for various optoelectronic devices such as ultrafast photodetectors,[6] solar cells,[7] and terahertz modulators.[8] It was demonstrated that graphene−metal contact-based photodetectors can operate with frequency up to 40 GHz,[6a] which is promising for high-speed optical communications.[6b] The photoresponse at the graphene−metal contacts was majorly attributed to the build-in electrical field arising from the work function difference at the graphene/metal interface.[9] Furthermore, photocurrent generations at the single-layer/bilayer graphene interface[9d] and dual-gated graphene p−n junctions[2,10] were observed afterward, and a hot-carrier-assisted photothermoelectric (PTE) effect was invoked to interpret the intrinsic photoresponse. Since the thermoelectric power of graphene can be easily tuned by the chemical potential and a considerable temperature gradient exists due to the inefficient cooling process of photoexcited hot electrons in graphene, hot-carrier-assisted photocurrent conversion is expected to be more efficient than the photovoltaic process.[2] Most recently, graphene was demonstrated to be able to convert a single absorbed photon into multiple hot electrons via an efficient carrier−carrier interaction.[11] This hot-electron multiplication effect, combined with broadband absorption and hot-carrier-assisted PTE effect, are essential ingredients for light harvesting and energy conversion.

The potential applications of graphene-based electronic and photonic devices further stimulated large-scale chemical vapor deposition (CVD) growth of intrinsic and heteroatom-doped graphene on various transition metals.[12] Recently, our group developed a modulation-doped growth method for the scalable synthesis of "mosaic graphene" consisting of single-crystalline lateral p−n junctions with spatially well-defined intrinsic and nitrogen-doped components (Figure S1). The photoresponse of a photodetector based on such p−n junctions was found to conform well to the PTE effect.[13] However, the conversion efficiency of graphene-based photodetectors seriously suffers from restrictions such as the relatively small area of the lateral p−n junction and the low light absorption of only 2.3% in single-layer graphene.[4] Several approaches have been developed to overcome the restrictions and improve the performance, such as integration of optical frequency antennas or plasmonic nanostructures,[14] optical microcavity[15] or waveguide[16] with photodetectors to increase the local optical intensity near the photoactive region. Nevertheless, such enhancement approaches are still hardly applied to traditional dual-gated graphene p−n junctions due to structural limitations of device configurations. Here we present the first realization of a plasmon-enhanced PTE conversion in CVD graphene p−n junction-based photodetectors coupled with gold plasmonic nanostructures.

Figure 1a demonstrates the schematic structure of a graphene p−n junction photodetector combined with gold plasmonic nanostructures. The nanostructures are expected to serve as optical antennas which convert the incident light into plasmonic oscillations and dramatically increase the electromagnetic field near the graphene p−n junction region (Figure 1b). The augmented production of electron−hole pairs in graphene excited by the intense near-field light will give rise to an enhanced photocurrent generation after the electron−hole pairs are separated due to the temperature gradient.

**Received:** May 21, 2013
**Published:** July 12, 2013



dx.doi.org/10.1021/ja404890n | J. Am. Chem. Soc. 2013, 135, 10926−10929

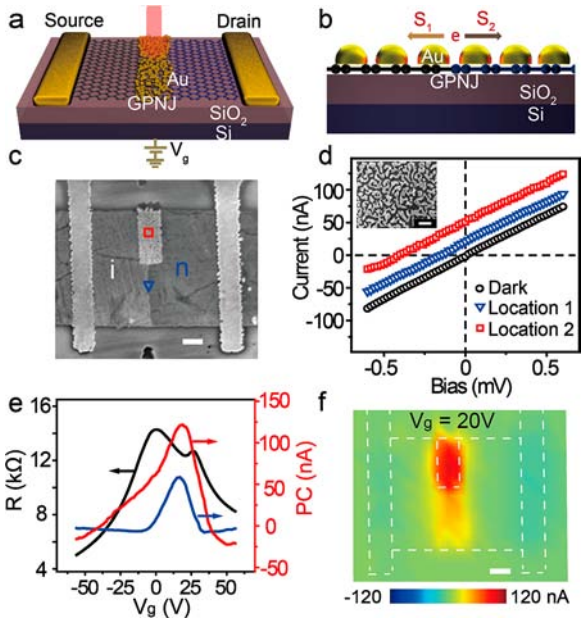


**Figure 1.** (a) Schematic drawing of a CVD graphene p−n junction (GPNJ) photodetector combined with gold plasmonic nanoparticles. (b) Photothermoelectric effect at the GPNJ with gold nanoparticles. Hot electrons diffuse with different Seebeck coefficients, $S_1$ and $S_2$. (c) SEM image of a device with the GPNJ partially covered with gold plasmonic nanostructures. Scale bar: 1 $\mu$m. (d) Current versus source−drain bias in the dark (black) and under the illumination of 633 nm laser beam focused at the GPNJ with (red) and without (blue) gold nanostructure covering. The illuminated areas are marked in (c). Inset is the high-resolution SEM image of the nanostructures in (c), which is composed of discrete irregular gold islands. Scale bar: 100 nm. (e) Photocurrent versus gate voltage with the laser focused at the above-mentioned two locations and transfer characteristic curve (black) of the device in the dark. (f) Photocurrent mapping image with the gate voltage set at 20 V. Scale bar: 1 $\mu$m.

Furthermore, hot electron−hole pairs arising from plasmon decay in the plasmonic metal may also take part in the PTE conversion process and further enhance the photoresponse.[14d]

CVD graphene p−n junctions were synthesized in a setup similar to our previous mosaic graphene work.[13] In general, monolayer graphene films consisting of lateral p−n junctions were first grown on copper foil by a modulation-doped growth method (see Methods in Supporting Information). The graphene film was then transferred using a "dry transfer" procedure[17] onto a $SiO_2$ (300 nm)/Si substrate. After that it was cut into graphene p−n junction strips via conventional electron-beam lithography (EBL) and oxygen plasma etching. Trilayer metals (0.5 nm Ti/25 nm Pd/20 nm Au) were deposited as source and drain electrodes followed by another lithography. Metal plasmonic nanostructures were then placed onto the graphene p−n junction area by transferring gold nanoparticles using poly(methyl methacrylate) (PMMA) film as a medium[14b] or directly annealing a thin gold film deposited by thermal evaporation.

Figure 1c shows a typical SEM image of a CVD graphene p−n junction device combined with gold plasmonic nanostructures. The intrinsic and N-doped graphene regions embedded in the device can be easily distinguished from the contrast: the brighter portion is intrinsic graphene, while the darker is N-doped graphene. The sharp and seamless junction is just right, located between the source and drain electrodes. Half of the p−n junction area is defined by EBL and deposited with a 4 nm thick gold film by thermal evaporation to carry out control experiments. After being annealed at 200 °C for 1 h in a forming gas atmosphere (20% $H_2$ and 80% Ar), the gold film agglomerated into discrete nanostructures (inset of Figure 1d) and formed a plasmonic enhancement region.[18] The Raman spectra of graphene underlying gold nanostructures excited with 632.8 nm laser can be strongly enhanced, indicating an effective plasmonic activity of as-prepared gold nanostructures (Figure S2). The representative transport properties of the CVD graphene p−n junction were investigated. The output and transfer characteristic curves of the as-grown p−n junction are presented in Figure 1, panels d (black circle) and e (black curve), respectively. Owing to the gapless feature of graphene, the $I-V$ curve of the CVD graphene p−n junction exhibited a non-rectifying behavior. Two maxima in the resistance-gate-voltage curve corresponded to the charge neutrality points of intrinsic graphene (28 V) and nitrogen-doped graphene (0 V), respectively (Figure 1e). The carrier mobility of intrinsic graphene (~4500 $cm^2\ V^{-1}\ s^{-1}$) and nitrogen-doped graphene (~2600 $cm^2\ V^{-1}\ s^{-1}$) extracted from the curve is relatively high, which is beneficial to the efficient photocurrent generation.

The PTE conversion of the CVD graphene p−n junction and its enhancement by the surface plasmon of metallic nanostructures were clearly observed under illumination. With a focused 632.8 nm laser beam (spot size, ~1 $\mu$m; power, 0.5 mW) illuminating at the CVD graphene p−n junction area without plasmonic nanostructures (marked with a blue triangle in Figure 1c), a pronounced shift of the $I-V$ curve occurred due to the generation of photocurrent as shown in Figure 1d (blue triangle). Meanwhile, the curve of photocurrent as a function of gate voltage at zero source−drain voltage exhibited a single peak with two polarity reversals as the gate voltage swept from negative to positive, as shown in Figure 1e (blue line). The shape of gate-dependent photocurrent was dominated by the PTE effect rather than photovoltaic effect, which can cause only a single sign change.[4,13,13]

When the laser was focused at the CVD graphene p−n junction area covered with plasmonic nanostructures (marked with red square in Figure 1c), the shift of the $I-V$ curve had a 2-fold increase in comparison with the photocurrent generated without plasmonic nanostructures (Figure 1d), indicative of the plasmonic enhancement of photocurrent generation. Moreover, such a photocurrent enhancement can be observed within the broad region of scanned gate voltages (Figure 1e). The achieved maximum photocurrent of the particular device increased 2-fold from 58 to 122 nA. It is noteworthy that the shape of the curve retained the two polarity reversals, which suggests that PTE effect still dominates the photocurrent conversion even when the plasmon resonance couples with the process of photocurrent generation.

We carried out spatially resolved photocurrent mapping to obtain more information about the plasmon-enhanced PTE conversion. As shown in Figure 1f and Figure S3, photocurrent maps were done with gate voltage fixed at −100, 20, and 60 V. Note that the photocurrent appeared in three separate zones: source, drain, and p−n junction area, which confirms that the gradient of doping level was necessary for the efficient separation of excited carriers in graphene. Photocurrent at the p−n junction area covered with plasmonic nanostructures was evidently stronger than that without plasmonic nanostructures. Especially when the gate voltage was fixed at 20 V, the


dx.doi.org/10.1021/ja404890n | J. Am. Chem. Soc. 2013, 135, 10926−10929

photocurrent at graphene p−n junction reached the maximum value and the plasmonic enhancement was most distinct.

It is of great importance to compare the plasmon enhancement effect of photocurrent generations at CVD graphene p−n junctions with that at graphene−metal junctions. To this end, we have transferred gold nanoparticles onto the whole device including both the graphene p−n junction area and electrodes.[14b] Briefly, gold nanoparticles with an average diameter of 115 nm and density of 28 particles/$\mu m^2$ were obtained by annealing an 8 nm gold film evaporated on a $SiO_2$/Si substrate at 350 °C in the forming gas (20% $H_2$ and 80% Ar). The nanoparticles were then transferred onto the target substrate with as-prepared devices using a spin-coated PMMA film as supporting layer, which is similar to the transfer process of graphene. After the PMMA was dissolved using acetone vapor, gold nanoparticles were left on the devices, as illustrated with the SEM image in Figure 2a. The plasmonic activity of the

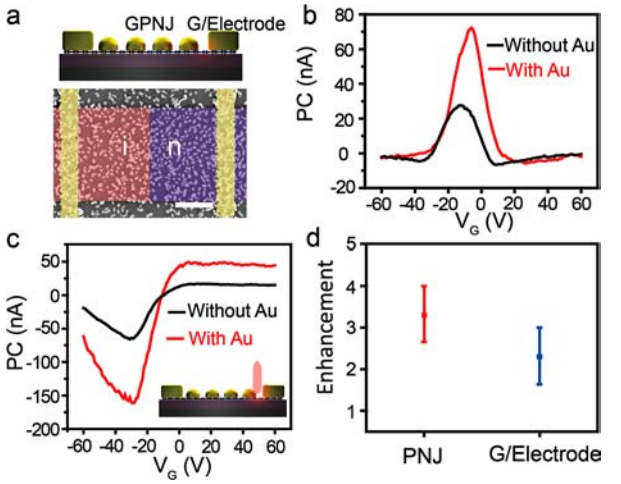


**Figure 2.** Comparison of the plasmonic enhancement factor between CVD graphene p−n junction (GPNJ) and graphene/electrode junction. (a) Bottom: false color SEM image of a GPNJ photodetector fully covered with transferred gold nanoparticles. Scale bar: 2 $\mu$m. Top: side view of the schematics of the device geometry. (b) Photocurrent versus gate voltage at GPNJ before (black) and after (red) transferring gold nanoparticles. (c) Photocurrent versus gate voltage at graphene/electrode before (black) and after (red) transferring gold nanoparticles. (d) Statistics of enhancement factors of GPNJ and graphene/electrode by plasmon resonance.

nanoparticles was confirmed by the extinction spectrum and the surface-enhanced Raman spectrum (SERS) of graphene (Figures S4 and S5). To evaluate the enhancement effect from different junctions, electronic properties and photocurrent were carefully measured in the same device before and after the transfer of nanoparticles. The transfer characteristics of the device changed little during the nanoparticle transfer process (Figure S6). Interestingly, significant enhancements of photocurrent and photovoltage responsivity were observed at both graphene p−n junction and graphene/electrode junction. Figure 2b,c presents typical gate-voltage-dependent photocurrents at the graphene p−n junction and the graphene/electrode junction, with the maximum photocurrent increased 2.6 and 3.0 times, respectively. Statistics of plasmonic enhancement factors in six other devices are shown in Figure 2d. The plasmonic enhancement factors of PTE conversion in graphene p−n junctions were 2.5−4.0 (Figure S7), while those of graphene−electrode junctions were 1.8−3.2. Correspondingly, the photocurrent responsivity of graphene p−n junction can be enhanced from 0.075 to 0.3 mA/W by plasmon resonance, while the photovoltage responsivity was enhanced from 1 to ∼4 V/W (Figure S8), which is comparable to the best results in the previously reported work.[2,14b,c] This observation indicated that the photocurrent and photovoltage enhancement factor of graphene p−n junction was comparable to that of graphene−metal junctions, which can be further increased by optimizing the shape and size of metallic nanostructures excited by incident light with a suitable wavelength.[14b−d] Indeed, we used gold nanoparticles with average diameters of 21, 115, and 220 nm, respectively, and found that the photocurrent generation was most strongly enhanced by 115 nm nanoparticles excited with 632.8 nm laser (Figure S9).

Graphene-based photodetectors traditionally require the illumination of a highly focused laser beam, which may restrict their practical applications. In order to produce non-zero net photocurrent with global illumination, metallic electrodes with different work functions are necessary for the fabrication of graphene photodetectors.[6b] However, it is possible to achieve the efficient photodetection or photocurrent conversion under global illumination in graphene p−n junction devices with symmetric metal contacts, especially when the photocurrent generation is enhanced by localized surface plasmon of metallic nanostructures. To this end, we placed gold plasmonic nanostructures on CVD graphene p−n junction area to fabricate a device capable of performing under global illumination (Figure 3a). Figure 3b shows the curves of gate-voltage-dependent photocurrent with the laser focused at source and drain electrodes and p−n junction area covered with gold plasmonic nanostructures, respectively. As expected, the photocurrent peak of the graphene p−n junction was much larger than that of the source and drain electrodes owing to the plasmonic enhancement. Note that the photocurrents

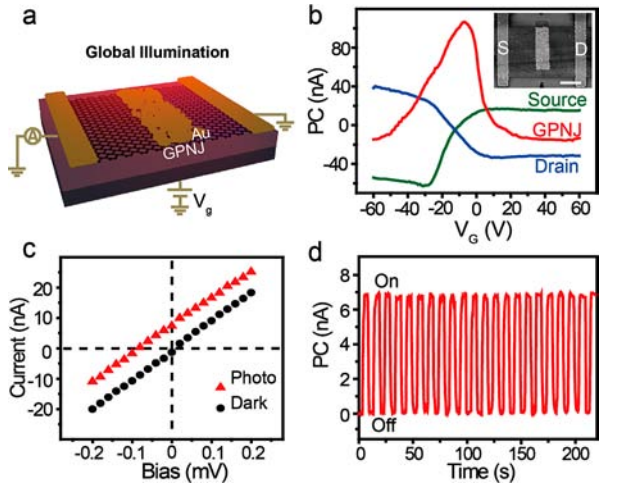


**Figure 3.** Global light photodetection via plasmonic enhancement of photothermoelectric conversion. (a) Schematic drawing of the detection of global light with the graphene p−n junction photodetector combined with plasmonic nanostructures. (b) Photocurrent contributions by a CVD graphene p−n junction and graphene/electrode junctions measured with the focused laser, respectively. Inset: SEM image of the CVD graphene p−n junction photodetector with the p−n junction area covered by gold plasmonic nanostructures. (c) Current versus source−drain bias in the dark (black circle) and with defocused 633 nm laser. (d) Time-dependent photocurrent generation with dynamic global laser illumination.


dx.doi.org/10.1021/ja404890n | J. Am. Chem. Soc. 2013, 135, 10926−10929

generated from source and drain electrodes were opposite at most gate voltages, but not totally antisymmetric since the Fermi levels of the two portions of graphene are different.[13] The overall photocurrent contributed by three different zones (graphene p−n junction and two graphene−metal junctions) was not zero; thus, photoresponse under global illumination was feasible. Indeed, a current shift of about 7 nA was observed when the whole device was globally illuminated by a defocused 632.8 nm laser (power, 0.2 mW; Figure 3c). Figure 3d shows representative switching cycles with zero source−drain bias when defocused laser was switched on and off repeatedly. A stable and repeatable operation of dynamic photoresponse was observed in such a global light photodetector. Meanwhile, the response time was found to be shorter than the current-measuring time of the equipment. It was reasonable to expect that the global light photodetector based on plasmon-enhanced graphene p−n junction was able to operate with ultrafast speed attributed to the high carrier mobility of graphene p−n junctions.[6]

In summary, we have demonstrated significant plasmonic enhancement of PTE conversion by the combination of CVD graphene p−n junctions with plasmonic nanostructures. The plasmonic enhancement factor of about 4 may be further improved with optimization of plasmonic nanostructures and the corresponding incident light. Global light photodetection with the plasmonic-enhanced PTE conversion was realized. The exploitation of plasmonic-enhanced PTE conversion is expected to promote the development of next-generation graphene-based high-efficiency optoelectronic devices.

## ■ ASSOCIATED CONTENT

### Supporting Information

Experimental details and supplementary figures. This material is available free of charge via the Internet at http://pubs.acs.org.

## ■ AUTHOR INFORMATION


### Corresponding Author

hlpeng@pku.edu.cn; zfliu@pku.edu.cn


### Notes

The authors declare no competing financial interest.

## ■ ACKNOWLEDGMENTS

We thank Prof. L. M. Qi for helpful discussions and acknowledge financial support by the National Natural Science Foundation of China (nos. 51121091, 51072004, 21173004, 21222303, 51290272) and the National Basic Research Program of China (nos. 2011CB921904, 2011CB933003, 2013CB932603, and 2012CB933404), NCET, and SRF for ROCS, SEM.

## ■ REFERENCES


(1) Britnell, L.; Gorbachev, R. V.; Jalil, R.; Belle, B. D.; Schedin, F.; Mishchenko, A.; Georgiou, T.; Katsnelson, M. I.; Eaves, L.; Morozov, S. V.; Peres, N. M. R.; Leist, J.; Geim, A. K.; Novoselov, K. S.; Ponomarenko, L. A. *Science* **2012**, *335*, 947−950.

(2) Gabor, N. M.; Song, J. C. W.; Ma, Q.; Nair, N. L.; Taychatanapat, T.; Watanabe, K.; Taniguchi, T.; Levitov, L. S.; Jarillo-Herrero, P. *Science* **2011**, *334*, 648−652.

(3) Chen, J. H.; Jang, C.; Xiao, S. D.; Ishigami, M.; Fuhrer, M. S. *Nat. Nanotechnol.* **2008**, *3*, 206−209.

(4) Nair, R. R.; Blake, P.; Grigorenko, A. N.; Novoselov, K. S.; Booth, T. J.; Stauber, T.; Peres, N. M. R.; Geim, A. K. *Science* **2008**, *320*, 1308−1308.

(5) Lee, C.; Wei, X. D.; Kysar, J. W.; Hone, J. *Science* **2008**, *321*, 385−388.

(6) (a) Xia, F. N.; Mueller, T.; Lin, Y. M.; Valdes-Garcia, A.; Avouris, P. *Nat. Nanotechnol.* **2009**, *4*, 839−843. (b) Mueller, T.; Xia, F. N. A.; Avouris, P. *Nat. Photonics* **2010**, *4*, 297−301.

(7) Wang, X.; Zhi, L. J.; Mullen, K. *Nano Lett.* **2008**, *8*, 323−327.

(8) Ju, L.; Geng, B. S.; Horng, J.; Girit, C.; Martin, M.; Hao, Z.; Bechtel, H. A.; Liang, X. G.; Zettl, A.; Shen, Y. R.; Wang, F. *Nat. Nanotechnol.* **2011**, *6*, 630−634.

(9) (a) Lee, E. J. H.; Balasubramanian, K.; Weitz, R. T.; Burghard, M.; Kern, K. *Nat. Nanotechnol.* **2008**, *3*, 486−490. (b) Xia, F. N.; Mueller, T.; Golizadeh-Mojarad, R.; Freitag, M.; Lin, Y. M.; Tsang, J.; Perebeinos, V.; Avouris, P. *Nano Lett.* **2009**, *9*, 1039−1044. (c) Park, J.; Ahn, Y. H.; Ruiz-Vargas, C. *Nano Lett.* **2009**, *9*, 1742−1746. (d) Xu, X. D.; Gabor, N. M.; Alden, J. S.; van der Zande, A. M.; McEuen, P. L. *Nano Lett.* **2010**, *10*, 562−566.

(10) Lemme, M. C.; Koppens, F. H. L.; Falk, A. L.; Rudner, M. S.; Park, H.; Levitov, L. S.; Marcus, C. M. *Nano Lett.* **2011**, *11*, 4134−4137.

(11) Tielrooij, K. J.; Song, J. C. W.; Jensen, S. A.; Centeno, A.; Pesquera, A.; Elorza, A. Z.; Bonn, M.; Levitov, L. S.; Koppens, F. H. L. *Nat. Phys.* **2013**, *9*, 248−252.

(12) (a) Reina, A.; Jia, X. T.; Ho, J.; Nezich, D.; Son, H. B.; Bulovic, V.; Dresselhaus, M. S.; Kong, J. *Nano Lett.* **2009**, *9*, 30−35. (b) Li, X. S.; Cai, W. W.; An, J. H.; Kim, S.; Nah, J.; Yang, D. X.; Piner, R.; Velamakanni, A.; Jung, I.; Tutuc, E.; Banerjee, S. K.; Colombo, L.; Ruoff, R. S. *Science* **2009**, *324*, 1312−1314. (c) Wei, D. C.; Liu, Y. Q.; Wang, Y.; Zhang, H. L.; Huang, L. P.; Yu, G. *Nano Lett.* **2009**, *9*, 1752−1758. (d) Reddy, A. L. M.; Srivastava, A.; Gowda, S. R.; Gullapalli, H.; Dubey, M.; Ajayan, P. M. *ACS Nano* **2010**, *4*, 6337−6342.

(13) Yan, K.; Wu, D.; Peng, H. L.; Jin, L.; Fu, Q.; Bao, X. H.; Liu, Z. F. *Nat. Commun.* **2012**, *3*, 1280.

(14) (a) Knight, M. W.; Sobhani, H.; Nordlander, P.; Halas, N. J. *Science* **2011**, *332*, 702−704. (b) Liu, Y.; Cheng, R.; Liao, L.; Zhou, H. L.; Bai, J. W.; Liu, G.; Liu, L. X.; Huang, Y.; Duan, X. F. *Nat. Commun.* **2011**, *2*, 579. (c) Echtermeyer, T. J.; Britnell, L.; Jasnos, P. K.; Lombardo, A.; Gorbachev, R. V.; Grigorenko, A. N.; Geim, A. K.; Ferrari, A. C.; Novoselov, K. S. *Nat. Commun.* **2011**, *2*, 458. (d) Fang, Z. Y.; Liu, Z.; Wang, Y. M.; Ajayan, P. M.; Nordlander, P.; Halas, N. J. *Nano Lett.* **2012**, *12*, 3808−3813.

(15) Engel, M.; Steiner, M.; Lombardo, A.; Ferrari, A. C.; Lohneysen, H. V.; Avouris, P.; Krupke, R. *Nat. Commun.* **2012**, *3*, 906.

(16) Liu, M.; Yin, X. B.; Ulin-Avila, E.; Geng, B. S.; Zentgraf, T.; Ju, L.; Wang, F.; Zhang, X. *Nature* **2011**, *474*, 64−67.

(17) Petrone, N.; Dean, C. R.; Meric, I.; van der Zande, A. M.; Huang, P. Y.; Wang, L.; Muller, D.; Shepard, K. L.; Hone, J. *Nano Lett.* **2012**, *12*, 2751−2756.

(18) Xu, W. G.; Xiao, J. Q.; Chen, Y. F.; Chen, Y. B.; Ling, X.; Zhang, J. *Adv. Mater.* **2013**, *25*, 928−933.